

---

# A Simple and Generalist Approach for Panoptic Segmentation

---

Nedyalko Prisadnikov<sup>1</sup>   Wouter Van Gansbeke\*   Danda Pani Paudel<sup>1</sup>   Luc Van Gool<sup>1,2</sup>  
<sup>1</sup> INSAIT, Sofia University   <sup>2</sup> ETH Zurich  
{firstname.lastname}@insait.ai

## Abstract

Generalist vision models aim for one and the same architecture for a variety of vision tasks. While such shared architecture may seem attractive, generalist models tend to be outperformed by their bespoke counterparts, especially in the case of panoptic segmentation. We address this problem by introducing two key contributions, without compromising the desirable properties of generalist models. These contributions are: (i) a positional-embedding (PE) based loss for improved centroid regressions; (ii) Edge Distance Sampling (EDS) for the better separation of instance boundaries. The PE-based loss facilitates a better per-pixel regression of the associated instance’s centroid, whereas EDS contributes by carefully handling the void regions (caused by missing labels) and smaller instances. These two simple yet effective modifications significantly improve established baselines, while achieving state-of-the-art results among all generalist solutions. More specifically, our method achieves a panoptic quality(PQ) of **52.5** on the COCO dataset, which is an improvement of 10 points over the best model with similar approach (Painter), and is superior by 2 to the best performing diffusion-based method Pix2Seq- $\mathcal{D}$ . Furthermore, we provide insights into and an in-depth analysis of our contributions through exhaustive experiments. Our source code and model weights will be made publicly available.

## 1 Introduction

In recent years, the computer vision community has witnessed a growing interest in developing generalist models that can tackle a wide range of tasks. This trend is inspired by the success of generalist models in Natural Language Processing (NLP), where a single, large model can effectively handle multiple tasks [2, 36, 1, 43, 44]. However, replicating this success in computer vision has proven challenging due to the inherent heterogeneity of the outputs. For example, outputs in computer vision can vary significantly, including categorical labels (classification) [10], bounding boxes [17], discrete segmentation maps [9, 13, 34], continuous pixel labels [41, 12], and more, posing a significant obstacle to consolidation. With the advent of more powerful image backbones [14, 4, 35, 26, 25, 16] generalist solutions have become better on a variety of tasks. Panoptic segmentation [19] remains one of the vision tasks where specialized solutions work better.

Panoptic segmentation is a dense prediction task that combines semantic and instance segmentation. It requires labeling each pixel of an input image with its corresponding semantic category as well as the specific instance to which it belongs. It tackles both *stuff-like* instance-less categories (like sky, grass, etc) and *thing-like* categories with one or more instances (people, cars, etc). State-of-the-art methods like [6, 22, 7, 53] achieve impressive results using transformer decoders with object queries [3]. Although these methods achieve impressive results, they are also highly specialized, i.e. cannot be easily applied to other tasks. Our work is inspired by Painter [49], which shows that many dense

---

\*Led the project while the author was at INSAIT. He is now affiliated with Google DeepMind.

vision tasks can be solved with a lightweight decoder on top of a powerful image encoder like [14], paired with a pixel-wise loss. It performs well on many tasks, but trails behind for the panoptic segmentation. We achieve competitive results by addressing the main limitations of this approach.

Instance segmentation is particularly challenging for generalist methods. The loss function must be invariant to a permutation of the instance labels. Specialized methods compute the loss by using Hungarian matching [21] to match predicted to ground-truth instances. This is done on a mask level. Performing Hungarian matching on the pixel level is very challenging. It requires clustering individual pixels into instances before performing the matching. This step is usually done in post-processing and involves computationally expensive non-maximum suppression algorithms. In Painter [49] the necessity of matching is removed by using deterministic instance label encoding based on the center of mass of the object. In other words each instance is uniquely labeled as a function of its center of mass. This allows for easy application of pixel-wise distance losses like  $L_1$  or  $L_2$ .

We follow the idea of regressing each pixel to the centroid of the instance it belongs to. However, we change the instance encoding using the spectral sine-cosine positional embeddings [47, 33] of the centroid coordinates  $u$  and  $v$ . Furthermore, we also show that when computing a pixel-wise loss for dense prediction tasks, it suffices to compute the loss on pixels near edges. In Section 4 we see that most of the limitations of this simple generalist approach to panoptic segmentation are related to various forms of imbalance and the additional care required for handling the missing labels.

This simple solution yields state-of-the-art performance among generalist methods for panoptic segmentation on MS-COCO [19]. We achieve this using a simple encoder-decoder architecture based on a vision transformer backbone encoder [35]. The very same backbone has already been shown to be useful for other dense prediction tasks like semantic segmentation and depth prediction [35, 25]. Our major contributions can be summarized as follows:

- **Spectral positional embeddings for the center of mass location.** Upto our knowledge, we are the first to use positional embeddings for the coordinate regression task. Instead of directly predicting the  $u, v$  coordinates of an instance’s center of mass, we predict their higher-dimensional representation based on sine-cosine positional embeddings. This helps equalize the distances between the encodings of different instances and tackles problems with data imbalance due to different scales of the loss in different image parts.
- **Edge distance sampling (EDS).** When averaging a per-pixel loss, we find that weighting each pixel contribution based on how far it is from an instance boundary, helps to resolve issues related to (i) natural data imbalance in images, and (ii) handling unlabeled regions.
- **Simple architecture.** We achieve our results with a simple architecture that is already used for other tasks. In fact, in terms of architecture, our solution does not differ from the semantic segmentation head used in [35].

We believe our simple but effective contributions are not limited to panoptic segmentation. Edge distance sampling can be useful for various other tasks. Using positional embeddings instead of direct coordinate regression addresses major challenges related to imbalance when using pixel-wise distance losses that are not scale-invariant, like  $L_1$  and  $L_2$ .

## 2 Related work

**Generalist vision models.** The recent trend in computer vision to build generalist models is driven by their success in the NLP field. Good examples of such vision models are [32, 49, 31]. Dense prediction tasks have often been tackled by powerful pre-trained image encoders like [4, 26, 25, 14] using fine-tuning with a simple tasks head. Often authors of such foundational models publish results with fine-tuned heads for tasks like semantic segmentation and depth prediction [35, 25]. We don’t aim to train a multitasking model similar to [32, 49], but to show that the challenging panoptic segmentation task [19] can be solved effectively in the general setup of a lightweight decoder on top of a powerful image encoder.

**Panoptic segmentation** is one of the more challenging dense prediction tasks for generalist models. We have to label each pixel with its semantic label, while additionally labeling each instance of *thing-like* objects with a unique instance id. Each permutation of the instance ids is also a valid answer.

This poses a challenge for generalist dense predictions models, especially ones that are trained with a pixel-wise loss. It is not clear how to compute the loss in this case. Specialized models [7, 6, 23, 53] use Hungarian matching [21] at instance level. It is challenging to make that work at the pixel level.

**Denoising diffusion methods.** Some methods resort to using denoising diffusion models to generate panoptic masks [5, 46]. During training, these methods generate the ground truth masks using random instance IDs with random noise added on top. The model learns to denoise the input. During inference the input to the model is random noise which results in the model assigning random instance ids. This prevents the need for Hungarian matching in the training loop.

**Deterministic instance encodings.** Before the advent of anchor/proposal based solutions like Mask-RCNN [15] and transformer methods based on DETR [3], a popular approach for solving the instance segmentation problem was using deterministic encodings for each instance ID. This allows for applying pixel-wise loss to check how close is the model prediction to the deterministic instance label. Examples of such encodings are ones based on the center of mass of the instance [49, 48], ones based on displacement to the center of mass [50], ones based on instance shape [52], etc. Our solution is based on encodings of the center of mass of the instances. This method has an additional desirable property, that it forces the model to learn about the whole object in order to be able to predict its instance label.

**Positional embeddings.** Positional embeddings (PE) has been a popular mechanism for dealing with the fact that the transformer is order-less since [47]. Additionally, they have been used to transform the input of coordinate MLPs (like NeRF [33]) to a higher-dimensional one [37, 51, 38]. We propose a novel way to use PEs as a replacement to direct coordinate regression.

### 3 Method

#### 3.1 Architecture and task setup

We solve the panoptic segmentation task in a multitasking setup, with two tasks: semantic segmentation and class-agnostic instance segmentation. A post-processing step combines the solutions of both tasks through majority voting of the semantic head for the predicted instances. For the *stuff* categories we only use the semantic segmentation output. Our architecture is similar to the one used in the DinoV2 [35] for the semantic segmentation task. We use DinoV2 as image encoder, with a lightweight decoder consisting of four transpose convolutional layers [29] to upscale the encoder image representation to the original image size. The encoder and decoder are shared between the two sub-tasks. Since the output dimension for each task is different, we use a task-specific head consisting of a *single convolutional layer* to transform to the correct dimension. See more details in Figure 1.

Let the input image be  $\mathbf{I} \in \mathbb{R}^{3 \times H \times W}$ . The output of the encoder is  $\mathbf{z} = f(\mathbf{I}) \in \mathbb{R}^{e \times H/p \times W/p}$ , where  $p$  is the patch size of the encoder transformer [11] and  $e$  is the embedding dimension throughout the encoder. The output of the shared decoder is  $\mathbf{h} = g(\mathbf{z}) \in \mathbb{R}^{d \times H \times W}$ , where  $d$  is the embedding dimension used in the decoder. Then the two task-specific heads map the  $d$ -dimensional embedding into semantic tensor  $\hat{\mathbf{y}}^{\text{sem}}$  and instance tensors  $\hat{\mathbf{y}}^{\text{inst}}$ , using a single convolutional layer.

#### 3.2 Pixel-wise loss with Edge distance sampling

For both of our semantic and instance prediction tasks, we compute simple pixel-wise losses. For the predictions  $\hat{\mathbf{y}}^{\text{inst}}$  and  $\hat{\mathbf{y}}^{\text{sem}}$ , we compute the following losses,

$$\mathcal{L}^t(\mathbf{y}^t, \hat{\mathbf{y}}^t) = \sum_{i=1}^H \sum_{j=1}^W w_{ij} L^t(\mathbf{y}_{ij}^t, \hat{\mathbf{y}}_{ij}^t),$$

where  $t \in \{\text{sem}, \text{inst}\}$ ,  $\mathbf{y}_{ij}$  is the  $(i, j)$  pixel in  $\mathbf{y}$  and  $w_{ij} \in [0, 1]$  is the corresponding weight for the loss, which is derived by using the method described below. For  $L^{\text{sem}}(\mathbf{y}_{ij}^{\text{sem}}, \hat{\mathbf{y}}_{ij}^{\text{sem}})$  on the semantic head, we use the standard cross-entropy loss on the predicted logits.

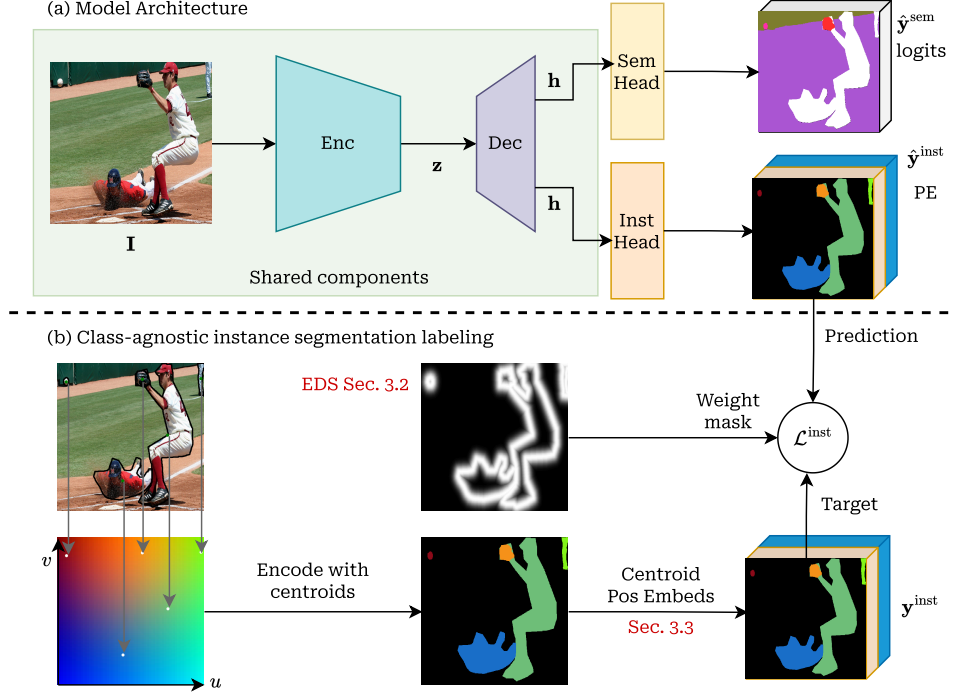


Figure 1: Overall model architecture (a) and handling of the class-agnostic instance segmentation task (b). The two tasks share both encoder and decoder. The task-specific heads are used only to map the decoded embedding  $h$  to the required dimensions. The color encoding of the instances through the centroids is for illustration purpose only. For instances, each pixel is encoded by its centroid location, followed by the positional embedding (PE). The instance head directly predicts PE.

**Edge distance sampling (EDS).** Although we compute a pixel-wise loss, we don't let all pixels contribute equally. We only train on pixels close to the object boundaries. For each pixel  $(i, j)$  we compute its euclidean distances  $d_{ij}$  to the nearest boundary. Then the weight of that pixel is derived using,

$$w_{ij} = w_{min} + (1 - w_{min})e^{-d_{ij}^2/D^2}.$$

Here  $w_{min}$  is the minimum weight for pixels that are far away from boundaries. In our experiments  $w_{min} = 0$ . The parameter  $D$  determines how quickly the weight decreases when going away from a boundary. In our experiments  $D = 20$ . See an example weight mask in Fig. 1 and 2.

The weight distribution in this manner helps us to focus on the image regions with the highest entropy. It is akin to lateral inhibition in human vision [28, 18], leading to the highest activations near edges. More importantly, it addresses two key problems of, (i) unlabeled regions by meaningfully discarding them; (ii) loss imbalance between small and large objects by focusing near to the instance edges. Please, refer Section 4 for the remaining discussion and details.

**Additional losses.** We use two additional losses, total variation loss [40] as a form of regularization and generalized DICE loss [8, 42]. More information about them can be found in Appendix A.

### 3.3 Positional embeddings for centroid regression

We tackle the class-agnostic instance segmentation task through encoding of the instances via their center of mass. In other words, for each pixel we predict the coordinates of the centroid of the corresponding instance. If a pixel does not belong to any labeled instance, we label it with a predefined *void* encoding. In this setting, the magnitude of the loss directly depends upon the precision of the predicted centroid. It is to be noted that the centroids are meant to serve as proxies for the clustering of a pixel, which otherwise has no significance for the task at hand. On the other hand, high precision in the centroid prediction is required on the boundary between instances with

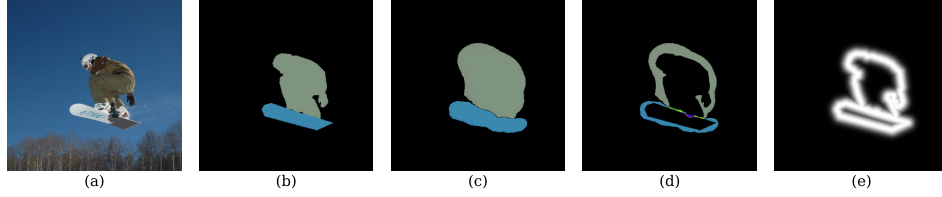


Figure 2: Instance expansion due to ignoring the void regions during training. The prediction (c) is much expanded compared to the target (b). The difference is shown in (d). A solution for this issue is the proposed Edge Distance Sampling (EDS). The weights obtained from EDS are shown in (e).

close centers of mass. This dichotomy hints us that the eventual mistakes in the instance predictions must be similarly treated – instead of penalizing based on “how far/bad” the predictions are. Please refer to an example in Fig. 4 and more details in Section 4.

To address the aforementioned issue, we propose to use the positional embedding of the centroid’s coordinates, mapping them to a higher-dimensional space in this process. We empirically show that this leads to a more equalized distances between center of masses, thereby penalizing the mistakes more fairly. In other words, the overall scale of the loss for mistakes in different parts of the image (and by different magnitudes of error displacements) becomes more equalized.

Let  $u$  and  $v$  be the coordinates of the center of mass of a given instance. We first normalize them to be values in the range  $[-1, 1]$ . Then we apply positional embeddings as used in [47, 33]. The final representation of each pixel for the class-agnostic instance segmentation task is given by,

$$\mathbf{y}_{ij}^{\text{inst}} = \begin{cases} \text{concat}(\gamma(u), \gamma(v)), & \text{if pixel } (i, j) \text{ belong to an instance with centroid at } (u, v) \\ \mathbf{0} \in \mathbb{R}^{4L}, & \text{if pixel } (i, j) \text{ is not labeled.} \end{cases}$$

The positional embedding  $\gamma$  is defined as,

$$\gamma(p) = [\sin(\pi p), \cos(\pi p), \sin(2\pi p), \cos(2\pi p), \dots, \sin(2^{L-1}\pi p), \cos(2^{L-1}\pi p)] \in \mathbb{R}^{2L},$$

where,  $L$  represents the number of harmonics we use and thus the dimensionality of the vector. The output  $\hat{\mathbf{y}}^{\text{inst}}$ , of the instance segmentation task head, is  $4L$ -dimensional vectors for each pixel.

The pixel loss for the instance segmentation task is computed as the average euclidean distance, between prediction and the target embeddings, of the  $u$  and  $v$  coordinates, which is given by,

$$L^{\text{inst}}(\mathbf{y}_{ij}^{\text{inst}}, \hat{\mathbf{y}}_{ij}^{\text{inst}}) = \frac{1}{2} \sum_{n=1}^2 \left\| (\mathbf{y}_{ij}^{\text{inst}} - \hat{\mathbf{y}}_{ij}^{\text{inst}})_{[2(n-1)L+1:2nL]} \right\|_2.$$

During the inference, the  $u$  and  $v$  coordinates are recovered from  $\hat{\mathbf{y}}_{ij}^{\text{inst}}$  using the nearest neighbor search method, between the prediction and a position in a discretized  $uv$ -grid space.

## 4 Rationale

We use a simple encoder-decoder architecture popular for other dense prediction tasks. Our contributions are agnostic to the architectural design choices. As can be seen from our experiments they perform very well on the panoptic segmentation task. The reason is that they address important limitations of the pixel-wise generalist approach. We introduce the limitations here and explain how we resolve them.

**Handling unlabeled regions.** This is a limitation for solutions with pixel-wise distance loss of the class-agnostic instance segmentation task. MS-COCO [24] do not have all instances labeled. Some regions of the images are unlabeled or *void*. These regions should be excluded when computing the loss. However, with methods using a pixel-wise distance loss, excluding the void regions means that we don’t teach the model where instances bordering unlabeled regions end. This leads the model’s predictions to expand instances where they border unlabeled *void* regions. You can see this in Fig. 2.

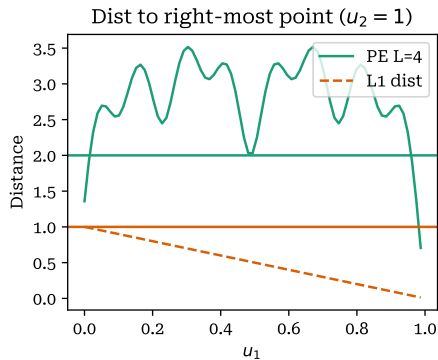


Figure 3: Showing the euclidean distances between the right-most point  $u_2 = 1$  and possible locations for  $u_1$  with positional embeddings. Also showing the  $L_1$  distance when regressing the value of  $u$  with PEs. The horizontal line depicts the distance from  $u_2 = 1$  and the encoding of the void region.

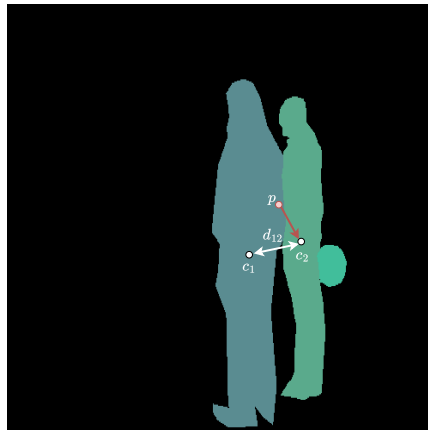


Figure 4: With centroid encoding of the instances, the scale of the loss for mistakes at the border between two instances depends on how far apart the two centroids are.

The model is incentivized to expand objects as much as possible in order to increase its confidence in the pixels in the inner parts of the objects.

Painter [49] – the approach for panoptic segmentation that comes closest to ours – treats unlabeled *void* regions as background and does not ignore them when computing the loss. This prevents the expansion issue, but wrongly penalizes the model when it predicts instances that are not labeled. When performing Edge distance sampling (Section 3.2) with  $w_{\min} = 0$ , we minimize the probability of such wrong penalization, while preventing the object expansion problem.

**Imbalance due to instance sizes.** One of the most common problems with models trained with a pixel-wise loss comes from imbalance. Imbalance can be caused by categories which are under-represented in the data, but it can also be caused by some categories having instances of a smaller size. An example of such imbalance is when the model’s loss is dominated by the small errors of already well predicted large objects, instead of by the large errors of poorly predicted small objects. This happens because large instances have more pixels and thus overwhelm the averaged loss.

Our edge distance sampling (Section 3.2) successfully minimizes the effect of imbalance due to object size. Intuitively, this is easy to understand by taking two circles as an example. Let us say the first circle has radius  $R$  and the second circle has radius  $2R$ . The ratio of the area of the two circles is  $1 : 4$ . Hence, the second circle contributes 4 times more to the loss. However, edge distance sampling mostly samples around the circumference of the two circles. Thus the contribution of the big circle will be roughly twice as large. Our experiments confirm this intuition. See Fig. 5 where we plot the average intersection-over-union(IoU) for different object sizes. As can be seen, edge distance sampling yields the biggest improvement for smaller objects.

**Imbalance due to difference in the scale of the loss.** Imbalance can also be caused if the scale of the loss is different at different parts of the images. For semantic segmentation we use cross-entropy loss which is scale invariant. However, for the instance segmentation task we use distance loss which is sensitive to the scale of the predicted values. Let’s look at this through an example (Fig. 4). With edge distance sampling we are only computing the loss on the boundary between two instances or the boundary between an instance and an unlabeled *void* region. In Fig. 4 point  $p$  is near the boundary of instances with centers  $c_1$  and  $c_2$ . If a point belonging to the first instance gets linked to the centroid of the second instance, the loss is the distance  $d_{12}$  between  $c_1$  and  $c_2$ . So, even if we are mistaken about instance adherence, the scale of the loss is determined by the distance between the instances’ centroids. It is interesting to note that small neighboring instances are more likely to have their centroids close to each other. So small instances which already contribute to the loss with fewer pixels, now contribute even less because the scale of the loss is smaller than for larger instances.

Method	Backbone	# Params	Image Size	PQ $\uparrow$
<i>Specialist methods:</i>				
Mask2Former [6]	Swin-L [26]	216M	$1024 \times 1024$	57.8
kMax-DeepLab [53]	ConvNeXt [27]	232M	$1281 \times 1281$	58.1
Mask DINO [23]	Swin-L [26]	223M	$1024 \times 1024$	<b>59.4</b>
<i>Generalist methods:</i>				
UViM [20]	ViT-Large [11]	939M	$1280 \times 1280$	45.8
Painter [49]	ViT-Large [11, 14]	370M	$448 \times 448$	41.3
LDM-Seg [46]	UNet [39]	851M	$512 \times 512$	43.3
Pix2Seq-D [5]	ResNet [16]	94.5M	$1024 \times 1024$	50.3
Ours	ViT-Base [35, 11]	91.9M	$420 \times 420$	48.6
Ours	ViT-Large [35, 11]	310M	$420 \times 420$	51.6
Ours	ViT-Large [35, 11]	310M	$518 \times 518$	<b>52.5</b>

Table 1: Panoptic segmentation results on MS-COCO [24]. Our method is the state-of-the-art among generalist methods. We use the ViT-Base model for the ablation study due to computational reasons.

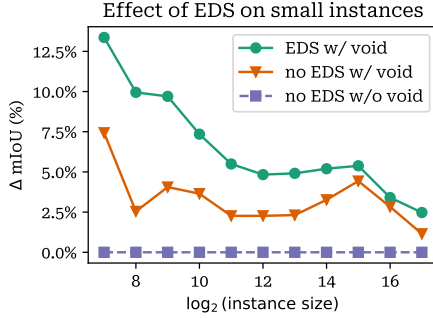


Figure 5: Effect of EDS on small instances. This charts shows that EDS has disproportionately bigger effect on smaller instances.

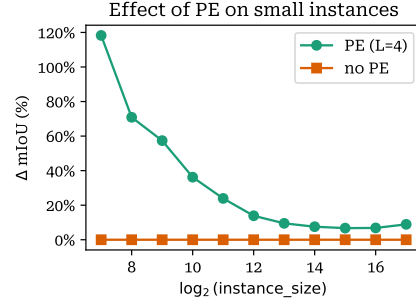


Figure 6: Effect of using PEs for the instance segmentation loss. It shows that PEs improve smaller instances more effectively.

Another interesting thing here is the fact that the largest boundary in the dataset is between an instance and a *void* region. So it is very important how we encode the void region and how far it is to other instances. If the void region is far away from the instances, this opens a potential imbalance where the boundaries between an instance and the void region dominate the loss. We saw this empirically when training models without positional embeddings. Boundaries between instances, especially if they are small, were much harder to learn, while learning the boundary between an instance and a *void* region was much easier. You can see this visually in Fig. 7.

Using positional embeddings instead of regressing to the centroid coordinates directly, helps mitigate these issues. In the higher dimensional space distances between vectors representing the positional embeddings are more equalized. A good example can be seen in Fig. 3. The plot takes into account only one coordinate (say  $u$ ) and plots the distance between  $u = 1$  (the right-most possible center-of-mass) and all other values of  $u$ . There is also a plot with the  $L_1$  distance in the case where we directly regress the value of  $u$ . The horizontal lines show the distance between  $u = 1$  and the encoding of the void region. With positional embeddings the void region is encoded as a vector of zeros. When using four harmonics ( $L = 4$ ) the void region is further away from  $u = 1$  than only a couple of other possible values for  $u$ . As discussed above this is desirable.

One important thing not visible from the plot is the contrast ratio, i.e. the ratio between the maximum and minimum distance from  $u = 1$  to any other centroid position. With the  $L_1$  loss without positional embeddings the contrast ratio is  $\approx 79$ . With positional embeddings ( $L = 4$ ) the contrast ratio is  $\approx 5$ .

EDS	Include void regions	PQ $\uparrow$
$\times$	$\times$	44.91
$\times$	$\checkmark$	46.74
$\checkmark$	$\times$	46.04
$\checkmark$	$\checkmark$	<b>48.61</b>

Table 2: Ablation on sampling the loss and ignoring the void regions. It shows the need to include *void* regions during training, where EDS helps to address the related issues.

Instance Encoding	PQ $\uparrow$
Direct centroid regression	41.61
Cross Entropy	39.87
Pos Embeds ( $L = 2$ )	46.58
Pos Embeds ( $L = 3$ )	47.38
Pos Embeds ( $L = 4$ )	<b>48.28</b>
Pos Embeds ( $L = 5$ )	48.12

Table 3: Ablation on using positional embeddings while regressing the centroids.

## 5 Experiments

### 5.1 Setup and implementation details

**Training setup.** We run our experiments on the MS-COCO dataset [24]. It contains 118K training images and 5K validation images. We adopt multitask implementation with the tasks being semantic and class-agnostic instance segmentation. Each batch contains only sampling from one of the tasks, with the instance segmentation being twice more likely.

We use DinoV2 [35] as a pretrained backbone, 12 layer DinoV2-Base for most of the ablation studies, and 24 layer DinoV2-Large for our best results. We don’t freeze the weight of the backbone, but use layer decay to suppress the learning rate of the earlier layers. The shared lightweight decoder consists of 4 upscale transposed convolutional layers [29]. It upscale the image to the original size. In most of our experiment the image size is  $420 \times 420$ , except for our best model where it is  $518 \times 518$ . The decoder takes input from four encoder layers - layers 3, 6, 9 and 12 when using DinoV2-Base, and layers 5, 12, 18 and 24 when using DinoV2-Large. Here we mirror the setup from DinoV2 [35] for the semantic segmentation task.

We train our model with effective batch size of 256, learning rate of  $5 \times 10^{-4}$  with linear warmup for 3 epochs, followed by cosine decreasing schedule [30]. Training lasts for 200 epochs or 92K steps.

Training for ablations is performed using DinoV2-Base backbone on a single node with  $8 \times A100$  GPUs. Training for 200 epochs takes less than 2 days. The large models using DinoV2-Large backbone are trained on a single node with  $8 \times H100$  GPUs. Training with image size  $518 \times 518$  using DinoV2-Large on the H100 GPU takes a little over 2 days.

We use Edge distance sampling (EDS) for both tasks with  $w_{\min} = 0$  and  $D = 20$ . For the class-agnostic instance segmentation we use positional embeddings with four harmonics,  $L = 4$ . We use total variation loss with weight 0.1. DICE loss is applied only for the instance segmentation task with weight of 1.

**Inference and evaluation.** Since our model produces a continuous output for each pixel we need to perform post-processing to get to the format of discrete masks. We follow a similar procedure as Painter [49], first performing non-maximum suppression (NMS) on the instance segmentation output, then majority voting within each instance for the semantic category. When processing the continuous outputs of the instance segmentation task, we discretize the possible center of mass location to a  $80 \times 80$  grid.

### 5.2 Panoptic segmentation results

We evaluate our method on the val2017 split of the MS-COCO dataset [24], and compare the results against two sets of SOTA methods - generalist and specialized. Our solutions using DinoV2-Large backbone achieves state-of-the-art among generalist methods, reaching PQ of 52.5 against 50.3 for the best diffusion based model Pix2Seq- $\mathcal{D}$ .

The method most related to ours is Painter [49] which is also trained with regression to the centroids with a pixel-wise loss. We achieve significant improvement over their score of 41.3 (43.4 for the multitasking model) even with a 12-layer encoder based on DinoV2-Base.



Our method still trails behind the specialized solutions, but we believe our work could be a stepping stone for future bridging of the gap. The contributions we demonstrate are general and architecture-agnostic, so they could possibly be used with future solutions for panoptic segmentation and beyond.

We notice an increase of **0.9** PQ only by increasing the input image size from  $420^2$  to  $518^2$ . This suggests we can expect further improvement of our solution with bigger increase of image resolution. We used the ViT based DinoV2 backbone as a proof-of-concept. It is computationally expensive and harder to scale to higher resolution. However, our method is encoder-agnostic so we can expect better scalability with alternative backbones.

### 5.3 Ablations

We perform our ablations using a DinoV2-Base backbone with image size of  $420 \times 420$ .

**Edge distance sampling.** Table 2 shows the ablations to evaluate the contribution of EDS. It shows we need to include the unlabeled *void* regions when computing the loss, and EDS is an effective way to minimize the issues coming from that. Additionally, Fig. 5 shows empirically that sampling only pixels near instance boundaries indeed has an effect on the imbalance due to object size. Using EDS has the biggest improvement on mean Intersection-over-Union (mIoU) for smaller objects. The experiments for this ablation are done using positional embeddings for the centroids with  $L = 4$ .

**Positional embeddings.** Table 3 shows how important it is to lift the centroid coordinates to a high-dimensional space using PEs. The model performs significantly better than using direct centroid regression or classification with cross-entropy loss. More details on how we evaluated direct centroid regression and classification can be found in Appendix B. The method based on cross-entropy performs very poorly, because the loss has no concept of distance. Fig. 6 shows that computing the loss within the space of positional embeddings brings even larger benefits for smaller instances, in addition to the EDS’ improvements. This ties in with our observation that smaller instances are more likely to have their centers of mass nearby. Thus, not only do they contain fewer pixels, but the scale of the loss for them also is likely to be small, when performing direct regression.

We found that using four harmonics ( $L = 4$ ) performs the best. The highest value we tried was  $L = 5$ , and it becomes computationally too expensive to go beyond.

## 6 Conclusion

In this paper we presented simple but effective solutions for the panoptic segmentation task, in the general and standard setup of finetuning a powerful image encoder with lightweight decoder and a pixel-wise loss. With this approach we achieve state-of-the-art performance on the COCO dataset [24] among generalist methods, with a significant improvement in performance. Such achievement is made possible by the proposed positional embedding based loss and edge distance sampling based weighting functions. We have provided a thorough discussion about these techniques, along with solid empirical evidences. While there is still a gap to specialized solutions, we hope that our contributions will be an important step towards closing this gap.

**Limitations and future work.** One limitation of our approach is that we generate continuous output for each pixel, despite the discrete nature of the instance masks. The final mask prediction still requires an additional post-processing step, which is desired to be within the training loop. One potential solution for this is to use quantization similar to vector quantization in VQ-VAE [45].

We use a DinoV2 backbone as a proof-of-concept for the panoptic segmentation task. The model despite performing very well is computationally expensive and hard to scale for larger image sizes. We briefly tried SWIN [26, 25], but found it hard to learn about center of mass without absolute positional embeddings in the transformer. Alternative backbones for scaling would be an interesting followup.

## **7 Acknowledgments**

This research was partially funded by the dAIedge project (HORIZON-CL4-2022-HUMAN-02-02, Grant Agreement Number: 101120726) and the Ministry of Education and Science of Bulgaria (support for INSAIT, part of the Bulgarian National Roadmap for Research Infrastructure).

## References

- [1] Josh Achiam, Steven Adler, Sandhini Agarwal, Lama Ahmad, Ilge Akkaya, Florencia Leoni Aleman, Diogo Almeida, Janko Altschmidt, Sam Altman, Shyamal Anadkat, et al. Gpt-4 technical report. *arXiv preprint arXiv:2303.08774*, 2023.
- [2] Tom Brown, Benjamin Mann, Nick Ryder, Melanie Subbiah, Jared D Kaplan, Prafulla Dhariwal, Arvind Neelakantan, Pranav Shyam, Girish Sastry, Amanda Askell, et al. Language models are few-shot learners. *Advances in neural information processing systems*, 33:1877–1901, 2020.
- [3] Nicolas Carion, Francisco Massa, Gabriel Synnaeve, Nicolas Usunier, Alexander Kirillov, and Sergey Zagoruyko. End-to-end object detection with transformers. In *European conference on computer vision*, pages 213–229. Springer, 2020.
- [4] Mathilde Caron, Hugo Touvron, Ishan Misra, Hervé Jégou, Julien Mairal, Piotr Bojanowski, and Armand Joulin. Emerging properties in self-supervised vision transformers. In *Proceedings of the IEEE/CVF international conference on computer vision*, pages 9650–9660, 2021.
- [5] Ting Chen, Lala Li, Saurabh Saxena, Geoffrey Hinton, and David J Fleet. A generalist framework for panoptic segmentation of images and videos. In *Proceedings of the IEEE/CVF International Conference on Computer Vision*, pages 909–919, 2023.
- [6] Bowen Cheng, Ishan Misra, Alexander G Schwing, Alexander Kirillov, and Rohit Girdhar. Masked-attention mask transformer for universal image segmentation. In *Proceedings of the IEEE/CVF conference on computer vision and pattern recognition*, pages 1290–1299, 2022.
- [7] Bowen Cheng, Alex Schwing, and Alexander Kirillov. Per-pixel classification is not all you need for semantic segmentation. *Advances in neural information processing systems*, 34:17864–17875, 2021.
- [8] William R Crum, Oscar Camara, and Derek LG Hill. Generalized overlap measures for evaluation and validation in medical image analysis. *IEEE transactions on medical imaging*, 25(11):1451–1461, 2006.
- [9] Gabriela Csurka, Riccardo Volpi, Boris Chidlovskii, et al. Semantic image segmentation: Two decades of research. *Foundations and Trends® in Computer Graphics and Vision*, 14(1-2):1–162, 2022.
- [10] Jia Deng, Wei Dong, Richard Socher, Li-Jia Li, Kai Li, and Li Fei-Fei. Imagenet: A large-scale hierarchical image database. In *2009 IEEE conference on computer vision and pattern recognition*, pages 248–255. Ieee, 2009.
- [11] Alexey Dosovitskiy, Lucas Beyer, Alexander Kolesnikov, Dirk Weissenborn, Xiaohua Zhai, Thomas Unterthiner, Mostafa Dehghani, Matthias Minderer, Georg Heigold, Sylvain Gelly, et al. An image is worth 16x16 words: Transformers for image recognition at scale. *arXiv preprint arXiv:2010.11929*, 2020.
- [12] Andreas Geiger, Philip Lenz, and Raquel Urtasun. Are we ready for autonomous driving? the kitti vision benchmark suite. In *2012 IEEE conference on computer vision and pattern recognition*, pages 3354–3361. IEEE, 2012.
- [13] Abdul Mueed Hafiz and Ghulam Mohiuddin Bhat. A survey on instance segmentation: state of the art. *International journal of multimedia information retrieval*, 9(3):171–189, 2020.
- [14] Kaiming He, Xinlei Chen, Saining Xie, Yanghao Li, Piotr Dollár, and Ross Girshick. Masked autoencoders are scalable vision learners. In *Proceedings of the IEEE/CVF conference on computer vision and pattern recognition*, pages 16000–16009, 2022.
- [15] Kaiming He, Georgia Gkioxari, Piotr Dollár, and Ross Girshick. Mask r-cnn. In *Proceedings of the IEEE international conference on computer vision*, pages 2961–2969, 2017.
- [16] Kaiming He, Xiangyu Zhang, Shaoqing Ren, and Jian Sun. Deep residual learning for image recognition. In *Proceedings of the IEEE conference on computer vision and pattern recognition*, pages 770–778, 2016.
- [17] Derek Hoiem, Santosh K Divvala, and James H Hays. Pascal voc 2008 challenge. *World Literature Today*, 24(1):1–4, 2009.
- [18] ME Jernigan and GF McLean. Lateral inhibition and image processing. In *Nonlinear Vision: Determination of Neural Receptive Fields, Function, and Networks*, pages 451–462. CRC press, 2018.

- [19] Alexander Kirillov, Kaiming He, Ross Girshick, Carsten Rother, and Piotr Dollár. Panoptic segmentation. In *Proceedings of the IEEE/CVF conference on computer vision and pattern recognition*, pages 9404–9413, 2019.
- [20] Alexander Kolesnikov, André Susano Pinto, Lucas Beyer, Xiaohua Zhai, Jeremiah Harmsen, and Neil Houlsby. Uvim: A unified modeling approach for vision with learned guiding codes. *Advances in Neural Information Processing Systems*, 35:26295–26308, 2022.
- [21] Harold W Kuhn. The hungarian method for the assignment problem. *Naval research logistics quarterly*, 2(1-2):83–97, 1955.
- [22] Feng Li, Hao Zhang, Huaizhe Xu, Shilong Liu, Lei Zhang, Lionel M Ni, and Heung-Yeung Shum. Mask dino: Towards a unified transformer-based framework for object detection and segmentation. In *Proceedings of the IEEE/CVF Conference on Computer Vision and Pattern Recognition*, pages 3041–3050, 2023.
- [23] Feng Li, Hao Zhang, Huaizhe Xu, Shilong Liu, Lei Zhang, Lionel M Ni, and Heung-Yeung Shum. Mask dino: Towards a unified transformer-based framework for object detection and segmentation. In *Proceedings of the IEEE/CVF Conference on Computer Vision and Pattern Recognition*, pages 3041–3050, 2023.
- [24] Tsung-Yi Lin, Michael Maire, Serge Belongie, James Hays, Pietro Perona, Deva Ramanan, Piotr Dollár, and C Lawrence Zitnick. Microsoft coco: Common objects in context. In *ECCV*, 2014.
- [25] Ze Liu, Han Hu, Yutong Lin, Zhuliang Yao, Zhenda Xie, Yixuan Wei, Jia Ning, Yue Cao, Zheng Zhang, Li Dong, et al. Swin transformer v2: Scaling up capacity and resolution. In *Proceedings of the IEEE/CVF conference on computer vision and pattern recognition*, pages 12009–12019, 2022.
- [26] Ze Liu, Yutong Lin, Yue Cao, Han Hu, Yixuan Wei, Zheng Zhang, Stephen Lin, and Baining Guo. Swin transformer: Hierarchical vision transformer using shifted windows. In *Proceedings of the IEEE/CVF international conference on computer vision*, pages 10012–10022, 2021.
- [27] Zhuang Liu, Hanzi Mao, Chao-Yuan Wu, Christoph Feichtenhofer, Trevor Darrell, and Saining Xie. A convnet for the 2020s. In *Proceedings of the IEEE/CVF conference on computer vision and pattern recognition*, pages 11976–11986, 2022.
- [28] Margaret S Livingstone. *Vision and art (updated and expanded edition)*. Abrams, 2022.
- [29] Jonathan Long, Evan Shelhamer, and Trevor Darrell. Fully convolutional networks for semantic segmentation. In *Proceedings of the IEEE conference on computer vision and pattern recognition*, pages 3431–3440, 2015.
- [30] Ilya Loshchilov and Frank Hutter. Sgdr: Stochastic gradient descent with warm restarts. *arXiv preprint arXiv:1608.03983*, 2016.
- [31] Jiasen Lu, Christopher Clark, Sangho Lee, Zichen Zhang, Savya Khosla, Ryan Marten, Derek Hoiem, and Aniruddha Kembhavi. Unified-io 2: Scaling autoregressive multimodal models with vision, language, audio, and action. *arXiv preprint arXiv:2312.17172*, 2023.
- [32] Jiasen Lu, Christopher Clark, Rowan Zellers, Roozbeh Mottaghi, and Aniruddha Kembhavi. Unified-io: A unified model for vision, language, and multi-modal tasks. In *The Eleventh International Conference on Learning Representations*, 2022.
- [33] Ben Mildenhall, Pratul P Srinivasan, Matthew Tancik, Jonathan T Barron, Ravi Ramamoorthi, and Ren Ng. Nerf: Representing scenes as neural radiance fields for view synthesis. *Communications of the ACM*, 65(1):99–106, 2021.
- [34] Shervin Minaee, Yuri Boykov, Fatih Porikli, Antonio Plaza, Nasser Kehtarnavaz, and Demetri Terzopoulos. Image segmentation using deep learning: A survey. *IEEE transactions on pattern analysis and machine intelligence*, 44(7):3523–3542, 2021.
- [35] Maxime Oquab, Timothée Darcet, Théo Moutakanni, Huy Vo, Marc Szafraniec, Vasil Khalidov, Pierre Fernandez, Daniel Haziza, Francisco Massa, Alaaeldin El-Nouby, et al. Dinov2: Learning robust visual features without supervision. *arXiv preprint arXiv:2304.07193*, 2023.
- [36] Alec Radford, Jeffrey Wu, Rewon Child, David Luan, Dario Amodei, Ilya Sutskever, et al. Language models are unsupervised multitask learners. *OpenAI blog*, 1(8):9, 2019.

- [37] Sameera Ramasinghe and Simon Lucey. Learning positional embeddings for coordinate-mlps. *arXiv preprint arXiv:2112.11577*, 2021.
- [38] Sameera Ramasinghe and Simon Lucey. A learnable radial basis positional embedding for coordinate-mlps. In *Proceedings of the AAAI Conference on Artificial Intelligence*, volume 37, pages 2137–2145, 2023.
- [39] Olaf Ronneberger, Philipp Fischer, and Thomas Brox. U-net: Convolutional networks for biomedical image segmentation. In *Medical image computing and computer-assisted intervention—MICCAI 2015: 18th international conference, Munich, Germany, October 5-9, 2015, proceedings, part III 18*, pages 234–241. Springer, 2015.
- [40] Leonid I Rudin, Stanley Osher, and Emad Fatemi. Nonlinear total variation based noise removal algorithms. *Physica D: nonlinear phenomena*, 60(1-4):259–268, 1992.
- [41] Nathan Silberman, Derek Hoiem, Pushmeet Kohli, and Rob Fergus. Indoor segmentation and support inference from rgbd images. In *Computer Vision—ECCV 2012: 12th European Conference on Computer Vision, Florence, Italy, October 7-13, 2012, Proceedings, Part V 12*, pages 746–760. Springer, 2012.
- [42] Carole H Sudre, Wenqi Li, Tom Vercauteren, Sebastien Ourselin, and M Jorge Cardoso. Generalised dice overlap as a deep learning loss function for highly unbalanced segmentations. In *Deep Learning in Medical Image Analysis and Multimodal Learning for Clinical Decision Support: Third International Workshop, DLMIA 2017, and 7th International Workshop, ML-CDS 2017, Held in Conjunction with MICCAI 2017, Québec City, QC, Canada, September 14, Proceedings 3*, pages 240–248. Springer, 2017.
- [43] Hugo Touvron, Thibaut Lavril, Gautier Izacard, Xavier Martinet, Marie-Anne Lachaux, Timothée Lacroix, Baptiste Rozière, Naman Goyal, Eric Hambro, Faisal Azhar, et al. Llama: Open and efficient foundation language models. *arXiv preprint arXiv:2302.13971*, 2023.
- [44] Hugo Touvron, Louis Martin, Kevin Stone, Peter Albert, Amjad Almahairi, Yasmine Babaei, Nikolay Bashlykov, Soumya Batra, Prajjwal Bhargava, Shruti Bhosale, et al. Llama 2: Open foundation and fine-tuned chat models. *arXiv preprint arXiv:2307.09288*, 2023.
- [45] Aaron Van Den Oord, Oriol Vinyals, et al. Neural discrete representation learning. *Advances in neural information processing systems*, 30, 2017.
- [46] Wouter Van Gansbeke and Bert De Brabandere. A simple latent diffusion approach for panoptic segmentation and mask inpainting. *arXiv preprint arXiv:2401.10227*, 2024.
- [47] Ashish Vaswani, Noam Shazeer, Niki Parmar, Jakob Uszkoreit, Llion Jones, Aidan N Gomez, Łukasz Kaiser, and Illia Polosukhin. Attention is all you need. *Advances in neural information processing systems*, 30, 2017.
- [48] Xinlong Wang, Tao Kong, Chunhua Shen, Yuning Jiang, and Lei Li. Solo: Segmenting objects by locations. In *Computer Vision—ECCV 2020: 16th European Conference, Glasgow, UK, August 23–28, 2020, Proceedings, Part XVIII 16*, pages 649–665. Springer, 2020.
- [49] Xinlong Wang, Wen Wang, Yue Cao, Chunhua Shen, and Tiejun Huang. Images speak in images: A generalist painter for in-context visual learning. In *Proceedings of the IEEE/CVF Conference on Computer Vision and Pattern Recognition*, pages 6830–6839, 2023.
- [50] Thomio Watanabe and Denis Wolf. Distance to center of mass encoding for instance segmentation. In *2018 21st International conference on intelligent transportation systems (ITSC)*, pages 3825–3831. IEEE, 2018.
- [51] Yiheng Xie, Towaki Takikawa, Shunsuke Saito, Or Litany, Shiqin Yan, Numair Khan, Federico Tombari, James Tompkin, Vincent Sitzmann, and Srinath Sridhar. Neural fields in visual computing and beyond. In *Computer Graphics Forum*, volume 41, pages 641–676. Wiley Online Library, 2022.
- [52] Wenqiang Xu, Haiyang Wang, Fubo Qi, and Cewu Lu. Explicit shape encoding for real-time instance segmentation. In *Proceedings of the IEEE/CVF international conference on computer vision*, pages 5168–5177, 2019.
- [53] Qihang Yu, Huiyu Wang, Siyuan Qiao, Maxwell Collins, Yukun Zhu, Hartwig Adam, Alan Yuille, and Liang-Chieh Chen. kmax-deeplab: k-means mask transformer. *arXiv preprint arXiv:2207.04044*, 2022.

## A Additional losses

As mentioned in the paper we use two additional losses to help us train a better model.

**Total variation loss** With edge distance sampling we don't include the inner parts of objects when computing the loss. Also, the output of our model is continuous prediction for each pixel. However, the desired output for both the semantic and class-agnostic instance segmentation tasks is discrete masks. This is why we use total variation loss [40] as a form of regularization. This loss is penalizing the model when the output of a given pixel is different from its neighbors. This is not desirable only for pixel that are at the border between different objects. The total number of such pixels is negligible. The definition of the total variation loss for a pixel  $i, j$  is as follows

$$l_{i,j}^{tv} = ||\mathbf{y}_{i,j} - \mathbf{y}_{i-1,j}|| + ||\mathbf{y}_{i,j} - \mathbf{y}_{i,j-1}||$$

Here  $\mathbf{y}_{i,j}$  is the output of the model for pixel  $i, j$ . The norm used depends on the main loss. If the main loss is  $L_1$  or  $L_2$ , the norm here is the same. For the instance segmentation task with positional embeddings the norm is the euclidean distance between the two embeddings.

When the main loss is cross entropy as in the semantic segmentation task, the total variation loss is defined as

$$\mathcal{L}_{tv} = \sum_{i=1}^{H-1} \sum_{j=1}^{W-1} \frac{1}{2} (\mathcal{H}(P_{i,j}, P_{i+1,j}) + \mathcal{H}(P_{i,j}, P_{i,j+1}))$$

where  $\mathcal{H}(a, b) = -a \log(b)$  and  $P_{i,j}$  is the probability distribution defined by the logits of the output for pixel  $(i, j)$ .

**DICE Loss** With edge distance sampling we ignore most of the unlabeled pixels when computing the loss, except in the globally applied total variation loss. This is good, because we don't know what is the correct label there. However, we know that whatever this label is it should not be the same as one of the already labeled instances. To enforce this we use a generalized DICE loss[42, 8]. This loss is an approximation of the mean intersection over union.

$$\mathcal{L}_{dice} = 1 - 2 \frac{\sum_l w_l \sum_{i,j} r_{l,(i,j)} p_{l,(i,j)}}{\sum_l w_l \sum_{i,j} (r_{l,(i,j)} + p_{l,(i,j)})}$$

Here,  $l$  is iterating over all labeled instances, while  $i, j$  are iterating over all pixels.  $w_l$  is the weight for each labeled instance. In our case  $w_l = 1/\text{Area}_l$ .  $r_{l,(i,j)}$  is the participation of pixel  $i, j$  to the instance  $l$  according to the ground truth, while  $p_{l,(i,j)}$  is the prediction of the fuzzy participation of pixel  $i, j$  to instance  $l$ .

$$r_{l,(i,j)} = \begin{cases} 1, & \text{if pixel } i, j \text{ belong to instance } l \\ 0, & \text{otherwise} \end{cases}$$

For the instance segmentation task with positional embeddings  $p_{l,(i,j)}$  is a score between 0 and 1, showing how likely the prediction for pixel  $i, j$  belong to instance  $l$ . Remember that  $\bar{\mathbf{y}}_{i,j} \in \mathbb{R}^{4L}$ . The first  $2L$  dimensions are the positional embedding of the  $x$  coordinate of the center of mass of the instance to which the pixel belongs. While the last  $2L$  dimensions are the positional embedding of the  $y$  coordinate. Let  $d_{i,j}^x$  and  $d_{i,j}^y$  be the euclidean distance between the ground truth and prediction for the embeddings of the  $x$  and  $y$  coordinates, respectively. Then,

$$p_{l,(i,j)} = e^{-(d_{i,j}^x)^2} e^{-(d_{i,j}^y)^2}$$

## B Alternative encodings for instance segmentation

Here we explained the alternatives we used to positional embeddings when regressing to the centroid for encoding the instances. There are two options, regression to the  $u, v$  coordinates of the centroid and classification with cross entropy loss.

**RGB encodings for centroid regression** Painter [49] used RGB encoding instead of directly predicting the coordinates of the centroid. He have a similar approach in out ablation study. We can directly regress to the  $u$  and  $v$  coordinates of the centroid, but then it is not clear how to encode the void pixels. Instead we use a 3-dimensional RGB encoding, where the red channel was equal the  $u$  coordinate of the centroid normalized to be in the region  $[0, 1]$ , the green channel was similarly equal to the  $v$  coordinate, and the blue channel was 1 only when the pixel was part of an instance. The encoding for the *void* pixels is pure black  $(0, 0, 0)$ . This is the method referred to as **Direct centroid regression** in Table 3.

**Cross entropy** We divide the image in  $80 \times 80$  grid cells and consider all centroids within a given cell to be the same. This allows us to solve the class-agnostic instance segmentation as a classification problem with 6400 categories. Performing this was too computationally expensive as we need 6400 logits for each pixel. Instead we classified independently the  $u$  and  $v$  coordinates of the center of mass into 80 classes. This is a much more computationally efficient solution. Performance is not good, because the cross entropy loss has no concept of distance. Thus small mistakes when the center of mass is challenging to compute, or when the ground truth mask is not precise, lead to problems with training.

## C Qualitative examples

Here, we show a few qualitative examples. Figure 7 shows the raw instance segmentation prediction of a model trained with direct centroid regression and a model trained with positional embeddings.

Figure 8 shows full model predictions, containing the raw semantic and instance segmentation outputs, and the result after post-processing in the last column.

## D Broader impact

Despite not achieving overall state-of-the-art result on the panoptic segmentation task, we believe that our work can bridge the gap between specialized and generalist models. Having better generalist models can lead to less harmful emissions from training multiple expensive models for different vision tasks. This work is only a stepping stone in this direction. Our contributions are very general and could lead to improvement in other areas of the Computer Vision community.

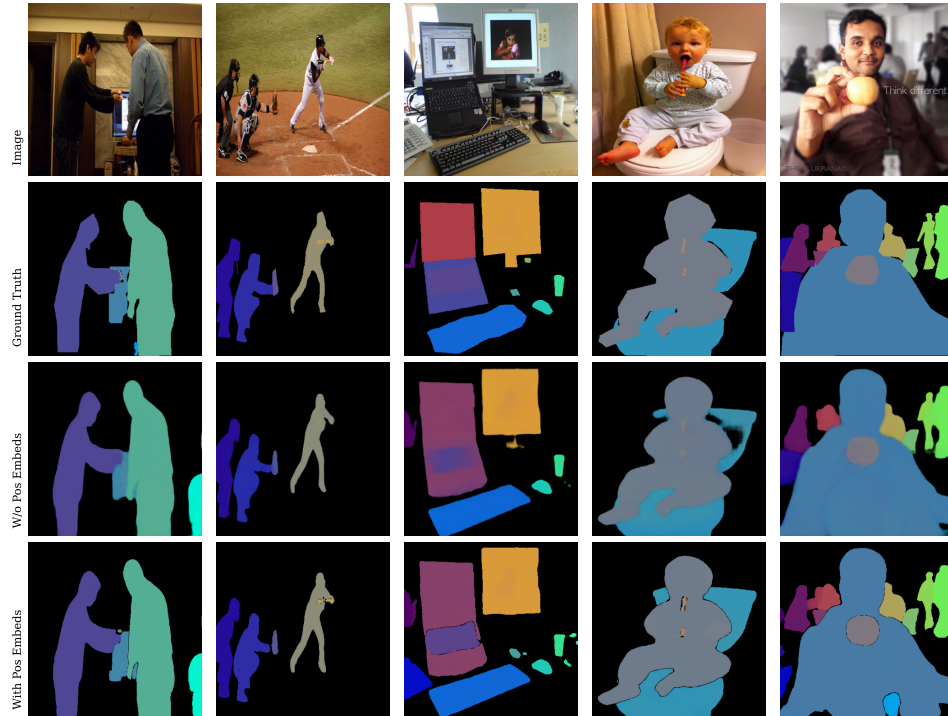


Figure 7: Comparing instance segmentation predictions with and without positional embeddings. It is clear how the boundaries between instances are much less blurry with positional embeddings. When training without positional embeddings the model learn the boundaries with void the best, but struggle with boundaries between objects, especially if the centers of mass are close. Both of these models are trained with DinoV2-Base backbone with image size  $420 \times 420$ .





Figure 8: Full examples from the COCO val dataset with semantic, instances and panoptic segmentation predictions. The semantic segmentation predictions are showing at each pixel the category with the highest likelihood. The instance segmentation show the nearest neighbor for the  $u, v$  coordinates applied to each pixel. The panoptic segmentation from the last column is the output of the post-processing step that combines the outputs of the semantic and class-agnostic instance segmentation heads.